# Post-failure behavior of Laminated Glass Beams

*Luigi Biolzi[a], Maurizio Orlando[b*], Lorenzo Ruggero Piscitelli[b], Marco Casucci[b] and Paolo Spinelli[b]*

[a] *Dipartimento di Architettura, Ingegneria delle Costruzioni e Ambiente Costruito, Politecnico di Milano, Milano, Italy*
[b] *DICEA: Dipartimento di Ingegneria Civile e Ambientale, Università degli Studi di Firenze, Firenze, Italy*

Prof. Eng. Luigi Biolzi, Full Professor of Structural Analysis and Design, Department of Architecture, Building Engineering and Built Environment, tel. +39.02.23994314, e-mail luigi.biolzi@polimi.it

Prof. Eng. Maurizio Orlando, Associate Professor of Structural Analysis and Design, Department of Civil and Environmental Engineering (DICEA), University of Florence, via di S. Marta 3, 50139 Florence (Italy) tel. +39.055.2758892 fax +39.055.2758800 e-mail maurizio.orlando@unifi.it

Eng. Lorenzo Ruggero Piscitelli, PhD student, Department of Civil and Environmental Engineering (DICEA), University of Florence, via di S. Marta 3, 50139 Florence (Italy) tel. +39.055.2758858 e-mail lorenzoruggero.piscitelli@unifi.it

Eng. Marco Casucci, Department of Civil and Environmental Engineering (DICEA), University of Florence, via di S. Marta 3, 50139 Florence (Italy) tel. +39.055.2758858 e-mail marco.casucci@unifi.it

Prof. Eng. Paolo Spinelli, Full Professor of Structural Analysis and Design, Department of Civil and Environmental Engineering (DICEA), University of Florence, via di S. Marta 3, 50139 Florence (Italy) tel. +39.055.2758885 fax +39.055.2758800, e-mail spinelli@dicea.unifi.it

[*] *corresponding author*

**Abstract**

In this paper an experimental investigation on the properties of progressively damaged laminated glass (LG) beams assembled with modified PVB interlayers is presented. It is well known that ionoplast interlayers significantly improve the load-bearing capacity, the dynamic response and the residual strength of damaged LG structural elements. These key elements in architectural glass design depend on the ability of the interlayer to grant adequate coupling effects between glass plies or the glass fragments. Therefore, it is important to test, model and understand the significant differences between LG beams laminated using different plastic materials. New interlayer polymers are being developed and gradually reach to the glass industry; reliable testing procedures are hence needed to assess benefits and differences among these materials. Since tempered glass has a remarkable tendency to expand when fractured, due to the formation of a large number of cracks, the volumetric increase has been studied and modelled from a macroscopic point of view, allowing to forecast the effect of shattered glass plies on the undamaged ones. The ‘‘tension stiffening” (TS) effect is a key element to understand the mechanical behavior of composite glass-interlayer elements. Studies of the TS effect and its evolution with time are needed for reliable post-breaking design and maintenance plan of damaged structures. Numerical models are discussed and validated to extend results to diverse types of laminated glass beam elements.

## 1 Introduction

The growth in the construction industry across the globe is anticipated to propel the market for construction glass in the next few years. Advancement in production and design technologies have made possible to build glass structures that are lighter and stronger than ever [1–3]. As the rising demand of glass elements drives the market, high load-bearing capacity, longevity and resilience are needed to bridge the gap from a mere architectural use of glass to proper and conscious structural applications.

Demands for application of glass in the construction industry usually exceed those required in other fields such as the automotive one [4], where transparency and post-failure safety are arguably the main concerns. For structural applications, the demand in term of safety has to cope with glass being a brittle material *par excellence* [5,6]. Under the right circumstances, glass plies can fail even by an arguably modest blow, therefore a thoughtful design of structural glass elements should also consider the event of glass failure. To improve the post-breakage behaviour of glass

elements, an efficient technique is to produce laminated glass (LG) by bonding together several plies with polymeric thermoplastic interlayers. The strong chemical bond to the interlayer prevents glass fragments from scattering in the event of glass failure. With keen and informed design, structural LG elements such as beams, columns, and floors can be created, overcoming the intrinsic safety limits of glass. On the other hand, the demand in terms of both longevity and structural resilience are related primarily to the properties of the interlayer itself and the strength of the adhesion bond with glass plies [7–9].

Safe design in building structures asks for reliable structures without the risk of catastrophic collapses. With brittle materials, such as glass, this safety is to be pursued via structural redundancy, that is the existence inside the structure of viable alternative load paths in case of failure of some structural elements. Multiple load path structures have this ability, and are often called "failsafe structures", while single load path ones have not, and are generally called "weakest link structures", because a suitable alternative load path is not present. For LG elements, required serviceability conditions need to grant that the failure of a glass ply does not turn out into a sudden and unanticipated collapse of the entire element or, most importantly, of the whole structure. Redundancy is related to the amount of functionality that the structure can sustain in the worst-case scenario of structural degradation. As a general idea for LG structures, the introduction of thermoplastic materials between glass plies allows for the element itself to have the required load bearing capacity until its substitution or evacuation (fail-safe response), while the rest of the structure is required to withstand the increased loads due to the local failure of one of its elements.

Glass has an elastic modulus that varies typically between 68 and 74 $GPa$ [10,11], while at room temperature any interlayer material has an elastic modulus that is three to five orders of magnitude lower [12]. These differences cause the composite material to behave in a peculiar manner [13]. Properties of the interlayer are very important in the undamaged glass phase [14], but even more in the post-breakage phase [15].

The performance of damaged LG elements is affected by the size and shape of glass fragments the strength of the adhesion bond and the stiffness of the interlayer. When one or more glass plies crack, they are unable to bear tensile stresses, so interlayers play a fundamental role in providing a residual load carrying capacity. Generally, the bigger size of glass fragments, the higher the stiffness: from a post-failure stiffness point of view, this condition should be viewed as an improved post-failure performance. Large fragments are typically produced by failure of annealed and toughened glass. Nonetheless, tempered glass is often used for LG in structural

applications [6,16] to achieve a higher surface tensile strength, and to enhance the performance of LG elements prior to failure. However, from a post-failure point of view, the tempering process might not be fully beneficial, as the small size of fragments produced by failure implies a greater effort of interlayers to grant the requested structural properties [17].

The most widely used polymeric films for glass lamination are: polyvinyl butyral (PVB) [18,19], Ethylene Vinyl Acetate (EVA) [20], SentryGlas (SG) [4,21] and DG41, a modified version of PVB, which has been introduced recently. Pure PVB requires the addition of softeners that gives plasticity and toughness; properties of EVA fluctuate from partial crystalline and thermoplastic to amorphous and rubber-like, but an amplified amount of vinyl acetate increases strength and ultimate elongation. SG is a ionoplast polymer primarily composed of ethylene/methacrylic acid copolymers with tiny amounts of metal salts; compared to PVB, SG exhibits both higher stiffness and strength. Nowadays, little is known on mechanical properties of DG41 itself and even less for DG41-glass laminates, this is the main reason driving the research towards a deeper understanding of properties of this interlayer material. All of the aforementioned interlayers are known to have critical temperature-dependent properties [12,22–24]. Post-failure analysis is crucial to assess the time interval for a partially or wholly damaged glass element to fail irreversibly under design loads. A number of relevant studies on the structural performance of architectural laminated glass elements [14,25–27], including lamination combined with embedded reinforcement [28], have been experimentally and numerically performed. Interesting studies on the behaviour of glass and glass-reinforced beams are also available [29–32].

For in-plane loading in the pre-failure phase, the interlayer has not any noteworthy influence on the flexural response due to the huge above-mentioned mechanical differences between the two materials. Nonetheless, the use of a stiff ionoplast interlayer significantly enhances the post-failure response [17]. In this paper, the tension-stiffening mechanism which arises once one or more glass plies break is discussed. Experimental tests were conducted on DG41 and DG41-reinforced LG beams, made with three fully tempered glass plies, to assess their post-failure behavior.

## 2 Setup and specimens

The experimental setup was designed to perform tests with increasing level of damage, starting from Undamaged Laminated Glass (ULG) specimens, down through Partially Damaged Laminated Glass (PDLG) specimens to Fully Damaged Laminated Glass (FDLG) ones, where all

glass plies have cracked. Tests were performed at the Laboratory of Structures and Materials of the Department of Civil and Environmental Engineering (DICEA) in Florence.

Three-layered laminated glass beams were assembled using 10 *mm* thick tempered glass plies, where 10 *mm* is to be intended as the commercial thickness, while the actual thickness measured at 100 edge points of beams ranges between 9.65 *mm* and 9.85 *mm*, with an average of 9.75 *mm* and a standard deviation of 0.05. No significant difference in the glass or interlayer thicknesses was observed between specimens of each series. A total of six specimens were provided, three of them were layered using 1.52 *mm* thick DG41 interlayers (DG samples), while the remaining ones were provided with a double 1.52 *mm* interlayer reinforced with a 0.2 *mm* thick polycarbonate foil (DGM samples). Cross-sections of beams are shown in *Figure 1*; once again, the total thickness is a nominal value, the actual one being slightly lower (32.29 *mm* and 35.53 *mm* on average for DG and DGM samples respectively).

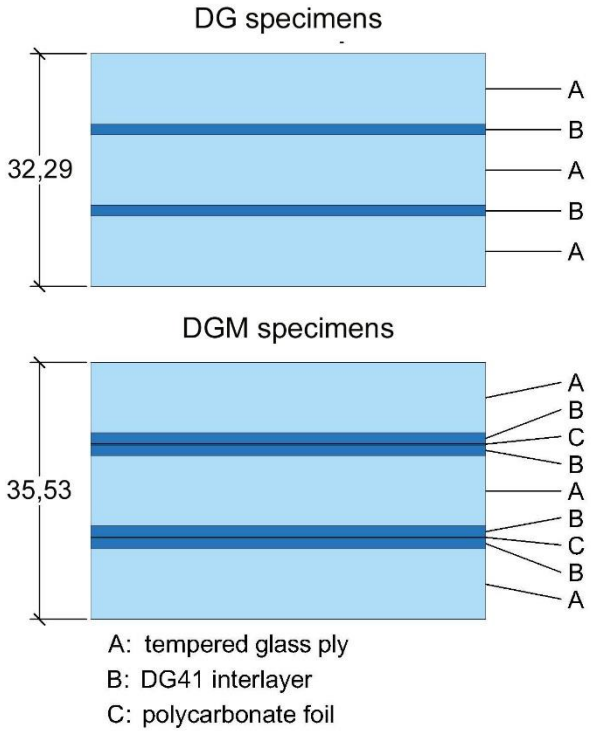


*Figure 1 - cross-sections of LG specimens*

The setup was designed to allow for the specimens to be simply supported at both ends on two steel rollers (Figure 2). Rollers were positioned on a 3560 *mm* long HE300B steel beam inserted on a MTS hydraulic press. The steel beam was bolted at midspan and supported near the ends by vertical struts. Safety lateral torsional restraints for the specimens were inserted close to supports rollers to avoid lateral-torsional buckling, but were not put in direct contact with the specimens.

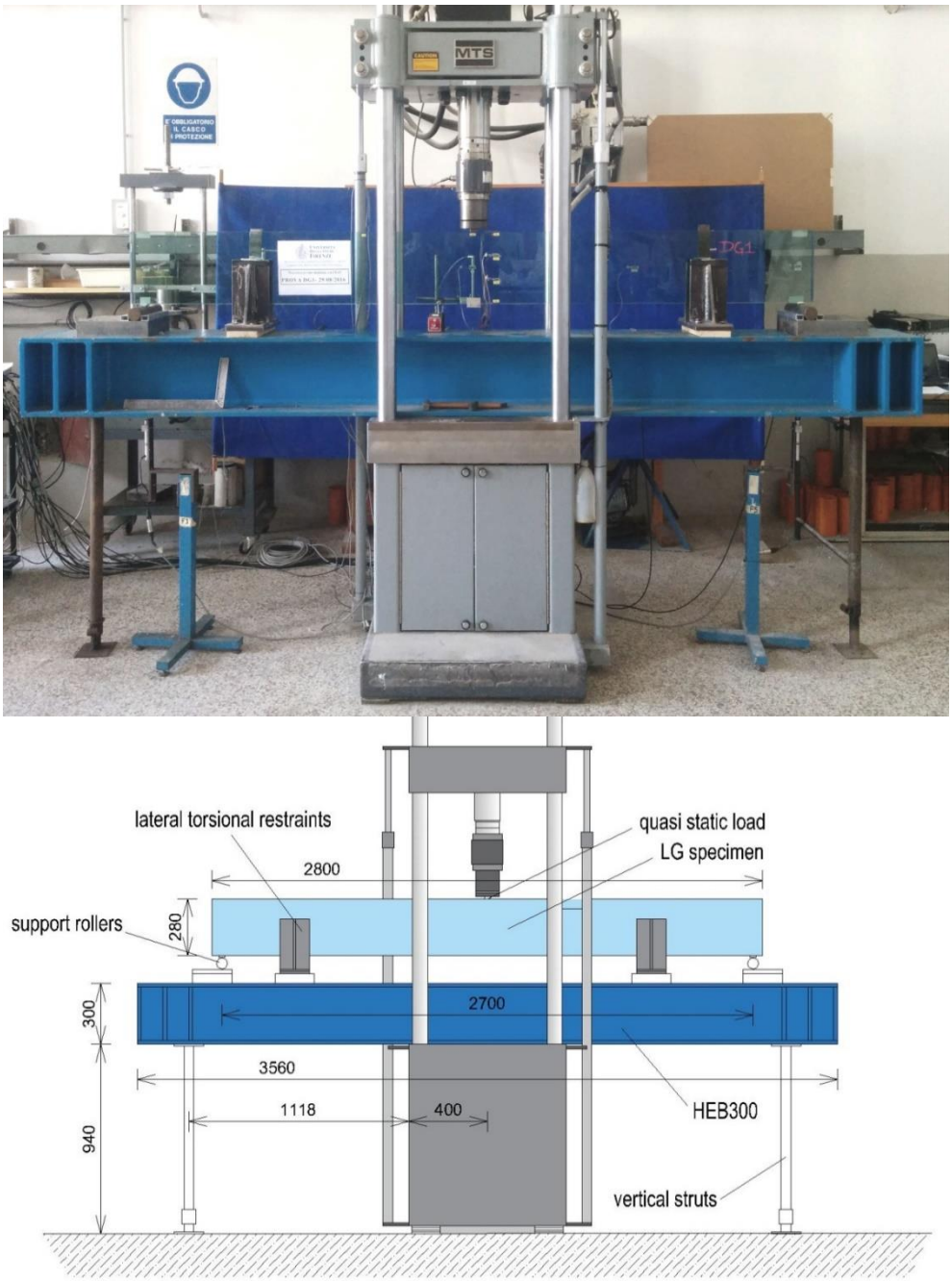


*Figure 2 – picture and lateral scheme of the setup*

To compensate small misalignments of glass plies and reduce friction between the specimen and supports, small aluminium pads were positioned between the specimen and rollers. As in all specimens there was not a perfect alignment between glass plies, a stiff epoxy resin was used to rectify the contact surface at both supports. In addition, a thick aluminium element was inserted between the top of the specimen and the hydraulic actuator to evenly spread the load among all the three glass plies, and a thin lead foil was inserted to compensate for eventual small misalignments of glass plies at mid-span.

## 2.1 Materials

The unit weight of each material was measured. After completing all tests on LG beam specimens with different damage levels (see § 3), glass fragments and interlayer stripes were extracted from FDLG specimens and following values of the unit weight were measured: $2{,}488 \pm 0.05\ g/cm^3$ for glass, $1{,}098 \pm 0.05\ g/cm^3$ for DG41, and $1{,}209 \pm 0.05\ g/cm^3$ for the polycarbonate foil, whose density was calculated by difference after assessing the density of the DG41 interlayer alone.

The thermoplastic interlayer used in the lamination process is a modified version of traditional PVB and it is known as DG41. This material is supposed stiffer than its traditional counterpart at room temperature, but data are not available for accurate design of LG elements using this interlayer material.

## 2.2 Monitoring and tests

Vertical displacements were monitored at midspan (F1 in Figure 3) and at both ends (F2 and F3). Specimens were also equipped with fifteen strain-gages, fixed to glass plies in several positions: in the section at 100 mm from the midspan (e1 to e10) and at five points along the axis on one of the two external plies (e11 to e15).

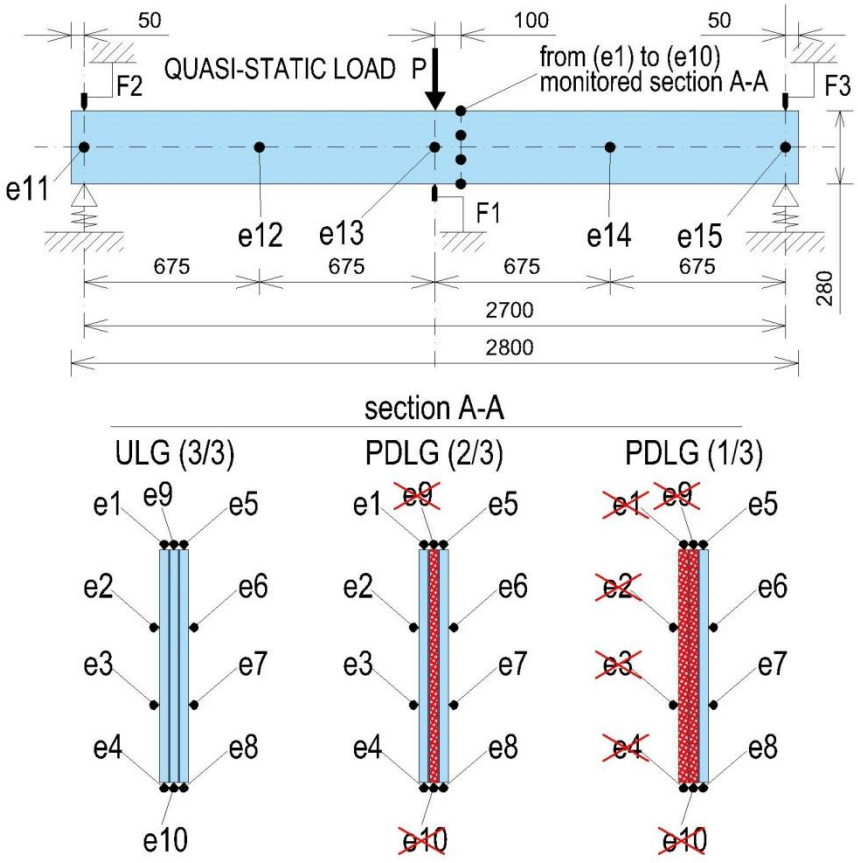


*Figure 3 - monitoring instruments for ULG and PDLG*

The instrumented section A-A was not chosen as the mid-span, but as close as possible to it, to avoid the influence of local effects induced by the load application at mid-span.

As the damage level increases, data from strain-gauges were progressively lost. Readings collected by strain-monitoring instruments connected to glass fragments are affected by the distribution of cracks. As the sheer number and aleatory distribution of crack can affect those instrument readings in several different ways, a general and reliable interpretation or model is a difficult task. Data originating from instruments on damaged plies have therefore not been considered.

The monitoring setup for FDLG tests had to be slightly adjusted to compensate for very high displacements and the loss of strain-gauge data. For the former problem, the displacement LVDT (Linear Variable Differential Transformer) at midspan (Figure 4a) was replaced by a potenziometer transducer (Figure 4b).

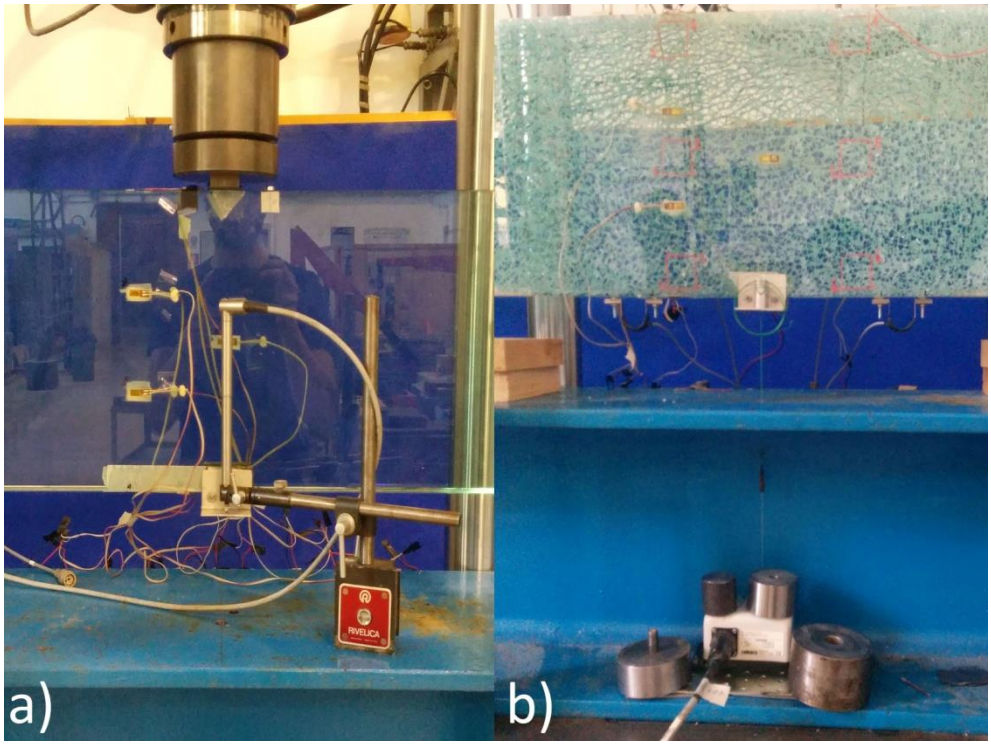


*Figure 4 - displacement transducer at midspan for a) ULG, PDLG and b) FDLG*

On the other hand, regarding the loss of strain-gauge measurements, four omega transducers were inserted adherent to the central - fractured - glass ply, as close as possible to the mid-span section (Figure 5). The confinement effect due to the presence of interlayer on both side of the glass fragments, together with the good adhesion between the two materials, allows to use the relative displacement readings of the base points of the omega transducers to compute the mean strain

between those points. Figure 6 shows one of the transducers, knowing the base distance $b_0 = 50\ mm$, the mean strain between the base points is $\bar{\varepsilon} = b/b_0$.

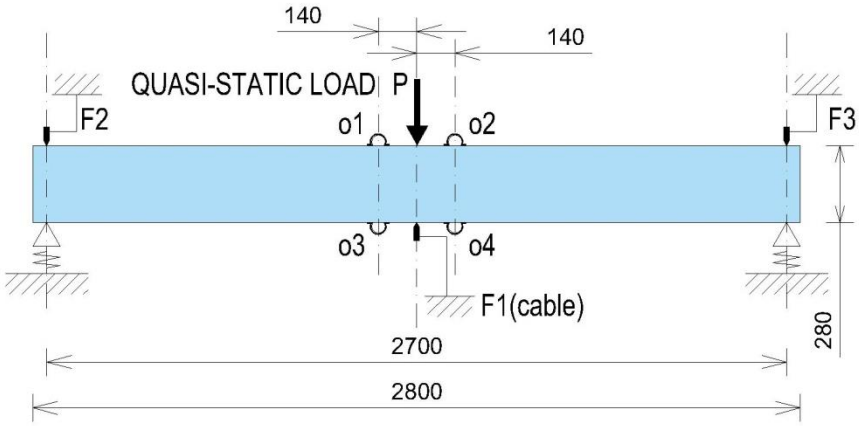


*Figure 5 - monitoring instruments for ULG and PDLG*

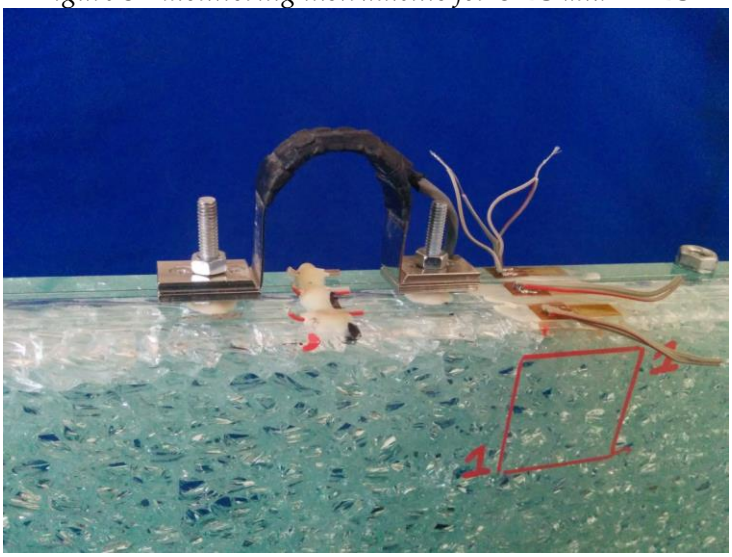

*Figure 6 - omega transducers installed for FDLG tests*

Several tests have been performed for increasing damage levels (Table 1).

*Table 1 - performed tests*

| Damage state | intact plies | test # | description |
|---|---|---|---|
| ULG | 3/3 | 1 | three-point bending test (0.01mm/s ramp up to 40 kN, hold 2 min and unload ramp, repeated twice) |
| PDLG | 2/3 | 2 | failure of the central ply and 24h strain monitoring |
| | | 3 | three-point bending test (0.01mm/s ramp up to 25 kN, hold 2 min and unload ramp, repeated twice) |
| | 1/3 | 4 | failure of the lateral ply and 24h strain monitoring |
| | | 5 | measure of the lateral sag at midspan |
| | | 6 | three-point bending test (0.01mm/s ramp up to 2.5 kN, hold 2 min and unload ramp, repeated twice) |
| FDLG | 0/3 | 7 | failure of the lateral ply (induced or flexural) |
| | | 8 | three-point bending test (0.1mm/s ramp up to 40 kN, hold 2 min and unload ramp) |

## 3 Experimental results

Experimental results are presented for increasing levels of damage.

### 3.1 Undamaged Laminated Glass

Mechanical properties of materials have been drawn from experimental tests. The Young modulus of glass, that according to European Standards ranges between 63 and 77 $GPa$ [11,33], has been obtained from flexural quasi-static tests on ULG, assuming that interlayers do not give any contribution (test #1, Table 1). For a simply supported LG beam of span $L$, composed by $n$ glass plies, each of thickness $t_g$ and moment of inertia $J_{1,g} = h^3 t_g/12$ about the strongest axis, under a concentrated load $P_m$ at mid-span, the elastic modulus of glass is given by:

$$E_g = \frac{1}{48} \frac{P_m L^3}{\eta_m n J_{1,g}}$$

Experimental values of $E_g$ have been evaluated on the loading plateau of 40 $kN$, held constant for two minutes, rather than during the loading and unloading phases. Tests on materials coming from different manufacturers yielded comparable results. Table 2 displays all experimental values of the glass elastic modulus, together with the elastic modulus of the thin polycarbonate layer [34,35]. The DG41 elastic modulus was assumed to vary between 10 and 1000 $MPa$.

*Table 2 – Values of the Young modulus of all materials assumed in FE models*

| material | manufacturer | specimen | experimental modulus $\boldsymbol{E}$ $[\boldsymbol{GPa}]$ | modulus E [GPa] used in FE models |
|---|---|---|---|---|
| glass | 1 | DG1 | 66.39 | 66.9 |
| | | DG2 | 65.83 | |
| | | DG3 | 68.45 | |
| | 2 | DGM1 | 66.69 | 67.8 |
| | | DGM2 | 67.71 | |
| | | DGM3 | 69.11 | |
| polycarbonate | 2 | DGM$x$ | 2.39 | 2.39 |
| DG41 | 1&2 | DG$x$ & DGM$x$ | - | 0.01,0.02,0.03,0.04,0.05,0.075 0.10,0.15,0.20,0.25,0.30,0.35 0.40,0.45,0.50,0.60,0.70,0.80,1.00 |

### 3.2 Partially Damaged Laminated Glass

A fictitious equivalent elastic modulus of a fractured glass ply was estimated from quasi-static tests on PDLG specimens, under the hypothesis that the cracked ply can still bear tensile stresses and its moment of inertia is the same as it was undamaged (Table 3). After a glass ply shatters, its adhesion to the interlayer still gives some contribution to the overall bending stiffness. Under the

hypothesis that shattered glass is still an isotropic material, the equivalent modulus for one ($E_{fg,eq,1}$) or two ($E_{fg,eq,2}$) shattered plies can be calculated as:

$$E_{fg,eq,1} = \frac{P_m L^3}{48 J_{1,g} \eta_m} - 2E_g$$

$$E_{fg,eq,2} = \frac{a P_m L^3}{96 J_{1,g} \eta_m} - \frac{E_g}{2}$$

where $a$ is a correction factor dependent on the position of torsional restraints, that only appears in tests with two broken plies, where the damaged beam is bent laterally and affected by torsional effects.

*Table 3 – fictitious equivalent Young modulus [GPa] of damaged glass plies*

| | **PDLG (2/3)** | | **PDLG (1/3)** | |
|---|---|---|---|---|
| | $E_{fg,eq,1}$ | **average** | $E_{fg,eq,2}$ | **average** |
| DG1 | 18.2 | | 16.7 | |
| DG2 | 16.3 | 18.9 | 15.3 | 15.2 |
| DG3 | 22.3 | | 13.6 | |
| DGM1 | 16.3 | | 9.09 | |
| DGM2 | 22.9 | 17.8 | 10.7 | 10.3 |
| DGM3 | 14.3 | | 11.0 | |

The hypothesis on the isotropy of shattered glass plies, bonded to one or two interlayers, is to some extent confirmed by experimental data. Readings of mid-span strain-gauges (e1 to e10 in Figure 3) are presented in Figure 7, for both loading ramps, of a specimen manufactured using DG1 interlayers, for different damage levels. Instrument readings have been reset at the beginning of each test, so results presented in Figure 7 do not account for strains induced by the failure of a glass ply on the others.

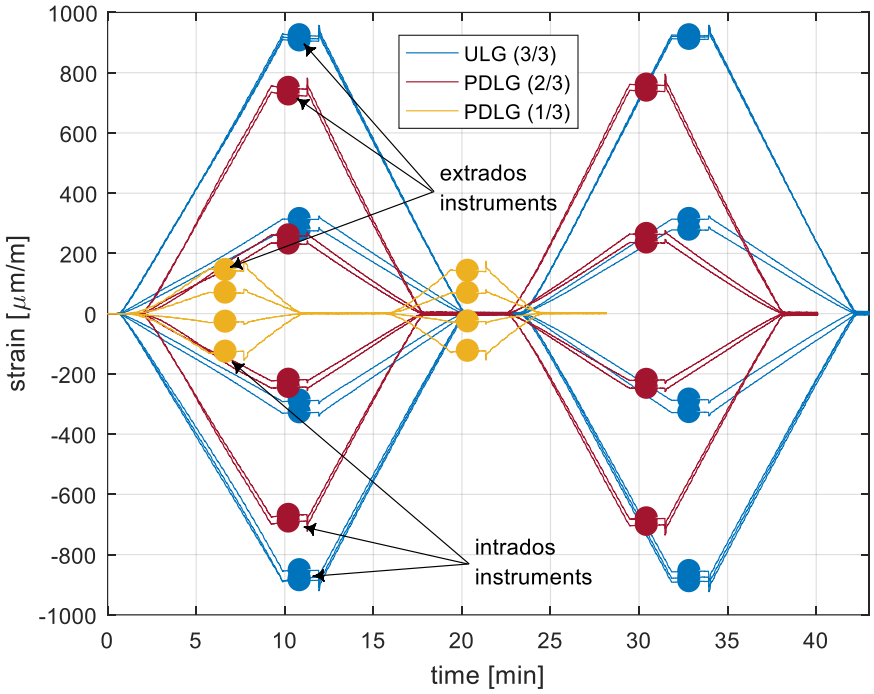


*Figure 7 – mid-span strain-gauge recordings for different damage levels*

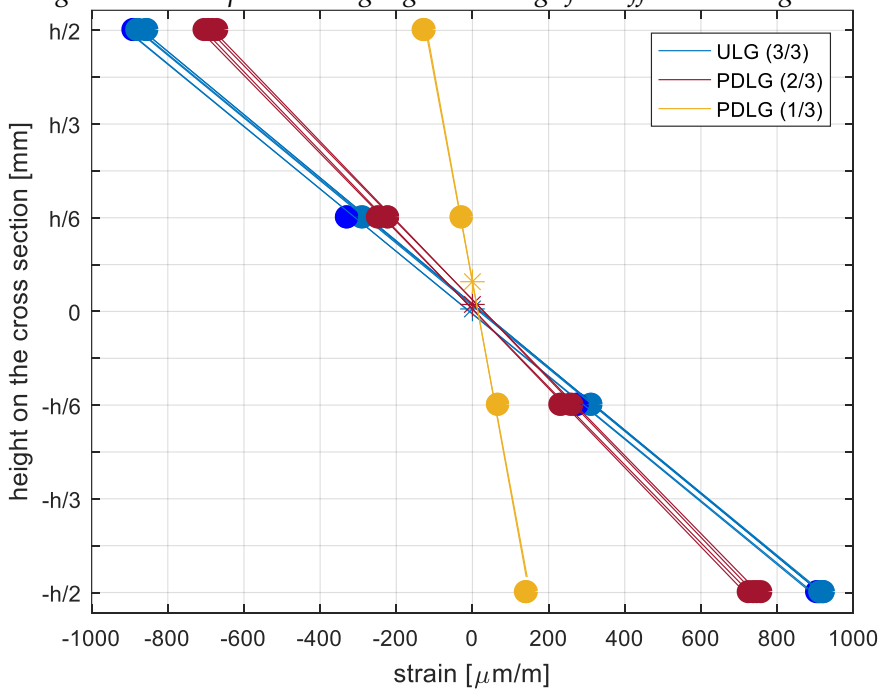


*Figure 8 - distribution of strains on the cross-section for different damage levels*

Figure 8 shows that the neutral axis is not significantly affected by the increase in damage in LG beams, and this appears to be true in all specimens, both for the DG*x* and DGM*x* series. The evolution of the neutral axis depth can be better understood by looking at results of the quasi-static bending test on specimen DGM2, which has been loaded up to the failure of the last glass ply (Figure 9).

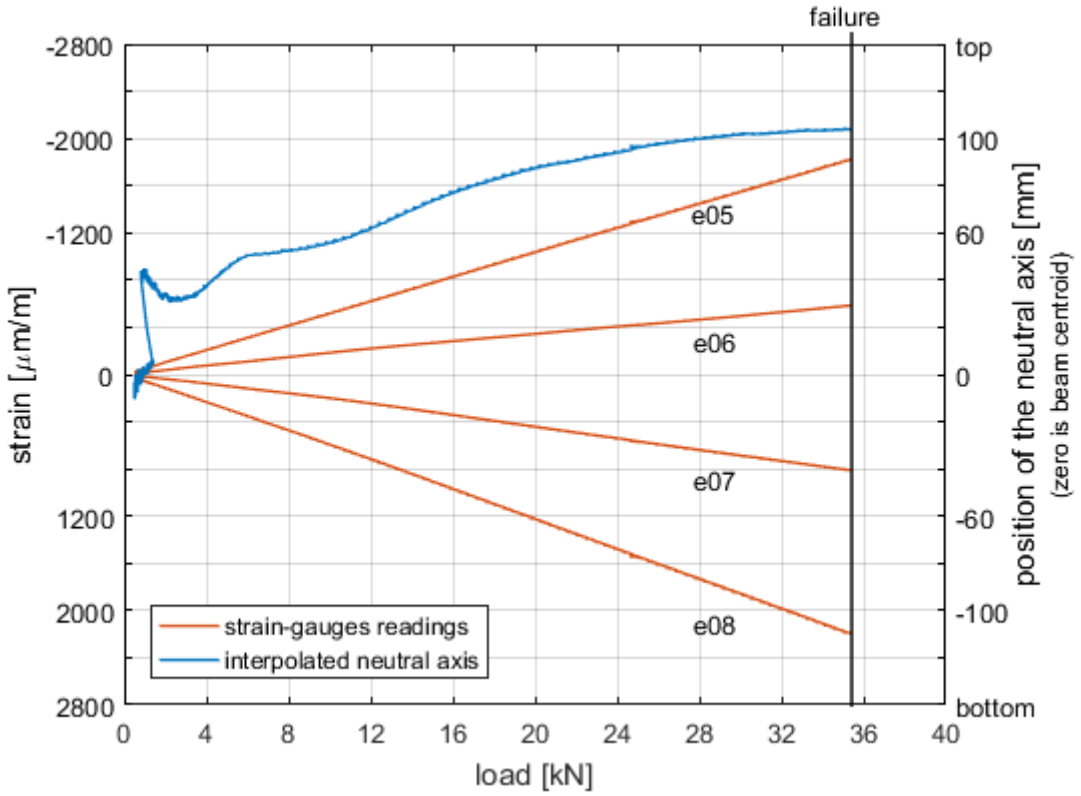


*Figure 9 - evolution of the neutral axis depth in specimen DGM2*

In all other tests, interpolated values of the neutral axis depth are given in Table 4, calculated at consistent load levels per each test.

*Table 4 – values of the neutral axis distance from the centroid [mm] for different damage levels*

| state | intact plies | DG1 | DG2 | DG2 | DGM1 | DGM2 | DGM3 | average DG*x* | average DGM*x* |
|---|---|---|---|---|---|---|---|---|---|
| ULG | 3 | 1,24 | 1,03 | 1,07 | 1,5 | 0,9 | 1,11 | **1,11** | **1,17** |
| PDLG | 2 | 3,48 | 3,1 | 3,38 | 3,11 | 3 | 3,32 | **3,32** | **3,14** |
| PDLG | 1 | 14,8 | 2,81 | 8,57 | 10,16 | 6,91 | 8,73 | **8,72** | **8,60** |

Results show that the neutral axis does not vary in a dramatic way at increasing the damage level. This result empowers the isotropic material hypothesis made for damaged glass plies and therefore allows with good confidence for the use of the equivalent stiffness results into the numerical model.

### 3.3 Finite Elements Models

Bending tests have been simulated with finite element (FE) models using ABAQUS [36] (Figure 10 and Figure 11). To avoid shear locking, 8-node solid elements with incompatible modes have been used for glass plies and hybrid solid elements with incompatible modes for interlayers. The choice

of a hybrid formulation for interlayer finite elements is connected to the inherent incompressibility of such polymers, whose Poisson coefficient $\nu$ is close to 0.5, generally $0.45 \leq \nu \leq 0.5$ [5,11].

The bond between glass plies and interlayers has been simulated via a kinematic constraint, preventing relative displacements at contact surfaces. On the other hand, to allow for shear sliding across the interlayer, three elements have been used through the thickness of the interlayer; lateral dimensions of these elements have been chosen lesser than 6 times their thickness [11].

Due to the symmetry of specimens, only half span of them has been modelled, and boundary constraints at mid-span have been defined to ensure the symmetry conditions. A FE model with a fine mesh has been assembled using 358,092 nodes and 264,282 elements (130,293 for each interlayer foil and 1,232 for each glass ply), while another FE model with a reduced mesh has been created using 24,201 nodes and 11,520 elements (4,836 for each interlayer foil and 616 for each glass ply), yielding an overall improvement of 93% in computational time.

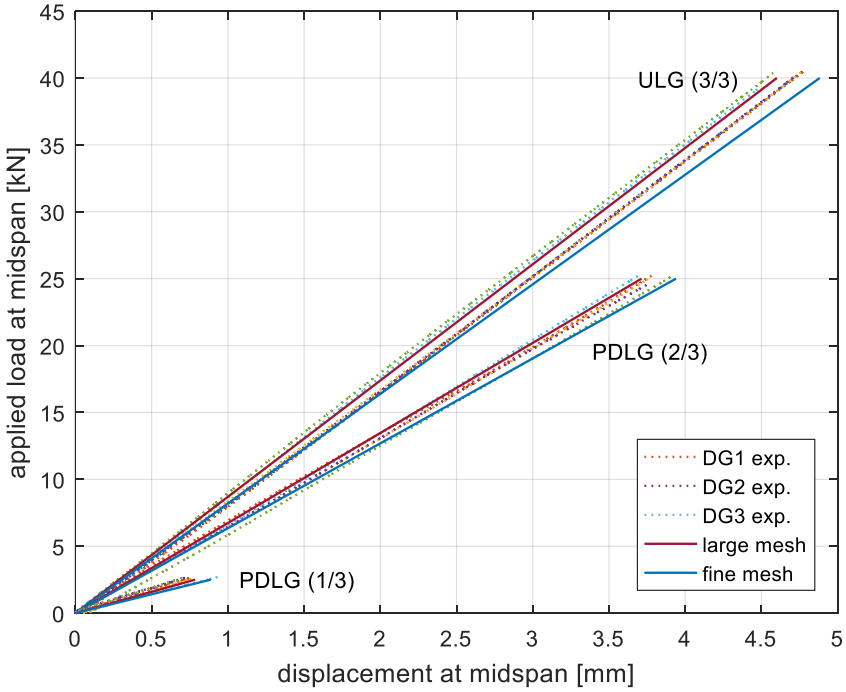


*Figure 10 – comparison of numerical and experimental load-displacement curves*

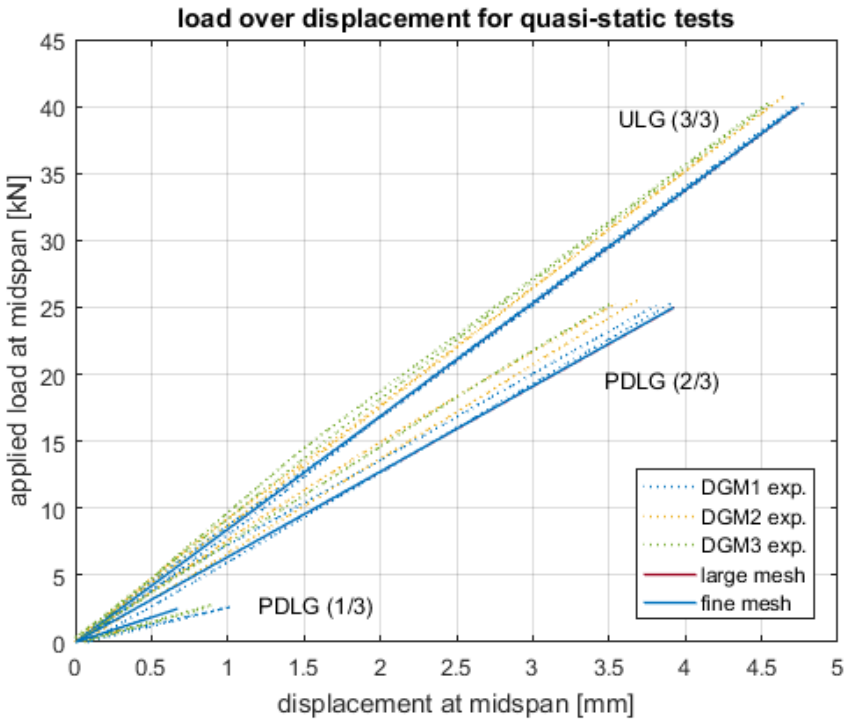


*Figure 11 – comparison of numerical and experimental load-displacement curves for reinforced LG*

### 3.4 Fully Damaged Laminated Glass

Failure of the last glass ply was artificially induced in all tests with a sharp edge, apart from the DGM2 specimen that was brought to failure under flexural loading. Bending tests on FDLG specimens were carried out at a significantly higher speed (mid-span displacement of 0.1mm/s) compared to other tests. Figure 12 shows data recorded for the FDLG DG2 specimen, where measured strains at the bottom and top of the beam on both sides of the mid-span allow for the depth of the neutral axis to be evaluated.

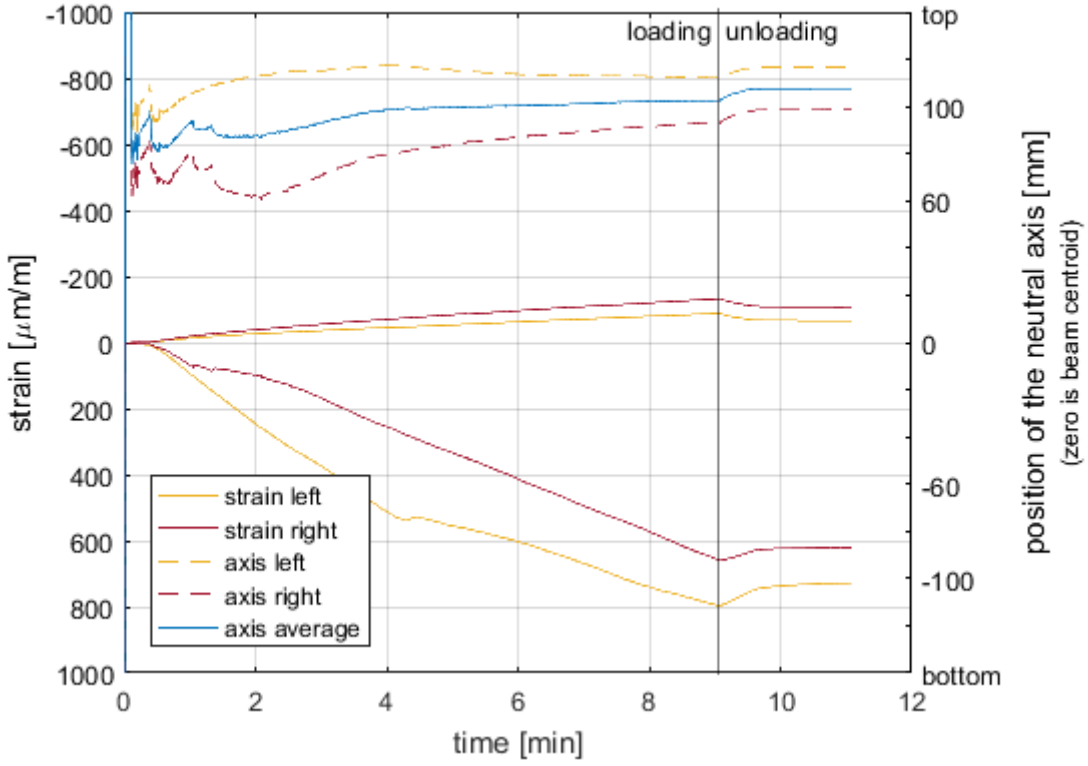


*Figure 12 – evolution of the depth of the neutral axis in the FDLG DG2 specimen*

The evolution of the depth of the neutral axis for other tests is shown in Figure 13. Note that data of the first specimen are not available, as omega transducers did not work properly during the test. For following tests, improvements were made to the measuring chain to allow for the whole test to be reliably monitored.

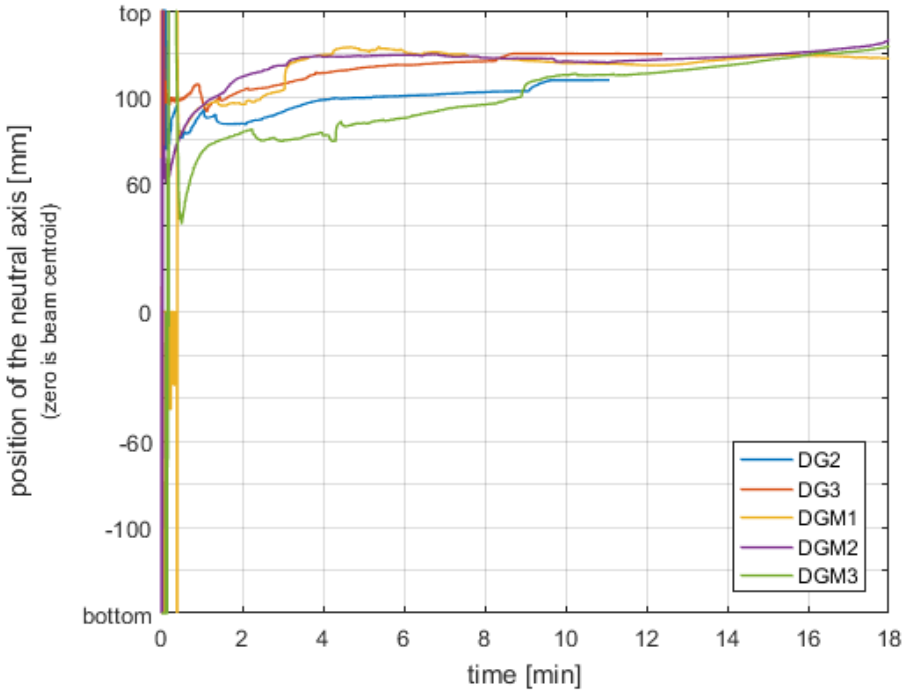


*Figure 13 - evolution of the depth of the neutral axis in all FDLG specimens*

In DGM-type specimens, the presence of a polycarbonate layer embedded in the interlayer material allowed for higher values of the load bearing capacity. Figure 14 shows results of three-point bending tests on FDLG specimens. The vertical axis shows the value of the mid-span bending moment $M_{n,m}$, normalized by the total interlayer thickness $t$ and accounting for the dead weight of the specimen:

$$M_{n,m}(\eta_m) = \frac{1}{t}\left[M_m^{P_m}(\eta_m) + M_m^d\right]$$

$$M_m^{P_m}(\eta_m) = \frac{P_m(\eta_m)L}{4}; \qquad M_{n,m}^d = \frac{MgL}{8}$$

where $M$ is the total mass of the specimen (glass plies + interlayers), $g$ is the standard gravity, and all other quantities have been introduced in previous sections.

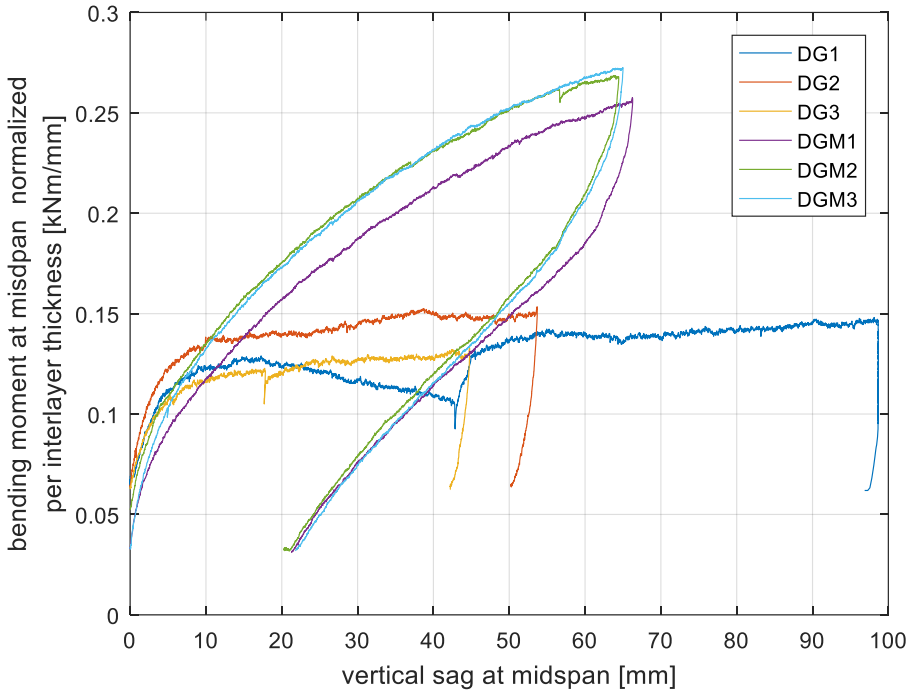


*Figure 14 – normalized bending moment over mid-span sag*

**Temperature equivalence for modelling glass failure**

Tempered glass has strong compressive stresses on outer surfaces and tensile stresses inside. For undamaged tempered glass, compressive and tensile stresses are in equilibrium; outer surfaces are plane and each portion exchanges equal and opposite actions with neighboring ones. Due to the elastic behavior of glass, when the glass fails, all fragments release part of the stored mechanical energy by expanding at the edges, releasing compressive stresses, and contracting in the central part, releasing tensile stresses. A simple explanation of this phenomenon is shown in Figure 15a.

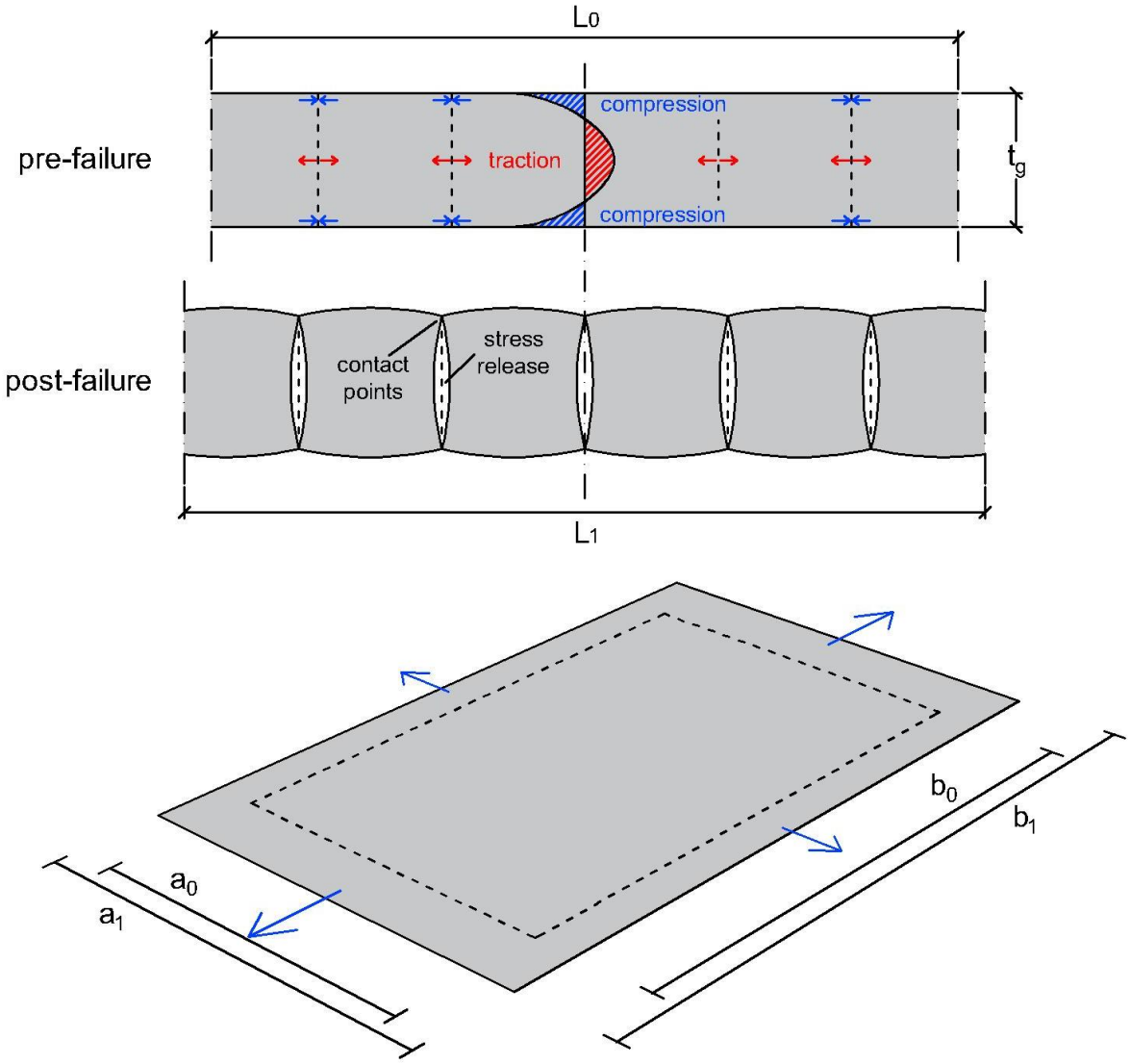


*Figure 15 - effect of the fragmentation of broken tempered glass plies*

If a system, like an interlayer with good adhesion, can keep fragments from scattering away, the observed macroscopic behavior of the fractured glass ply is its tendency to expand in its own plane. The expansion illustrated in Figure 15b is arguably not easy to model starting from a microscopic point of view, as the exact repulsion mechanisms are dependent on a variety of factors such as the strength and depth of the tempering process, the thickness of the glass ply, cracks density and distribution, shape of fragments, size of contact points between fragments, etc.

For PDLG elements, to simulate mutual effects of broken tempered glass plies on undamaged ones, which should be the primary concern for a structural engineer in a post-failure design, the authors have reproduced the volume increase, produced by the onset of cracks, by means of an equivalent non-isotropic temperature gradient (i.e. a numerical gradient only applied in the directions of the beam length and width). With this assumption, one can postulate that, if the interlayer shear stiffness is zero, the fractured glass increases in size freely without affecting

adjacent glass plies (Figure 16a). If the hypothesis that plane sections remain plane still holds [37], the solution to the problem can be found with the flexibility method (or method of consistent deformations) as presented in Figure 16.

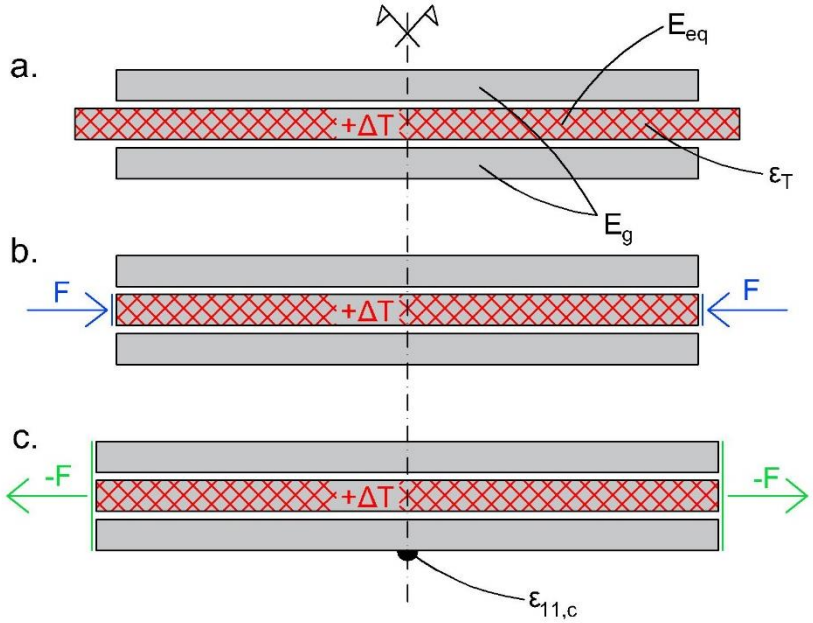


*Figure 16 - model for an expanding central fractured glass ply using the flexibility method*

The equivalent temperature variation $\Delta T_{eq}$ can be defined as a function of the fictitious equivalent modulus $E_{fg,eq}$ of the fractured glass ply. If the axial stiffness of the interlayer is negligible compared with any of the glass plies, fractured or not, and provided the experimental measure of the axial strain on the lateral – undamaged – glass ply, it follows that:

$$\Delta T_{eq}(E_{fg,eq}) = \frac{1}{\alpha_g}\left(\frac{A_g}{A_{fg}}\frac{E_g}{E_{fg,eq}} + 1\right)\varepsilon_{11,c}$$

where $E_g$ is the Young modulus of glass, $A_g$ and $A_{fg}$ are the cross-sectional areas of undamaged glass and fractured glass, respectively, $\alpha_g = 90 \cdot 10^{-7} K^{-1}$ [10,11,38] is the thermal expansion coefficient for glass, $\varepsilon_{11,c}$ is the measured strain in the longitudinal direction at mid-span on the outer undamaged plies upon failure of the central ply.

$\Delta T$ values have been calculated considering values of $E_{fg,eq}$ of PDLG specimens with one or two broken plies (

Table 5); this procedure is only meant to be accurate for symmetric damage states, so it is just approximate for the non-symmetric damage state with two broken plies.

*Table 5 - equivalent modulus and gradient for PDLG models*

| Damage state | intact plies/total | symmetric | $E_{fg,eq}$ $[MPa]$ | $\Delta T_{eq}$ $[K]$ |
|---|---|---|---|---|
| PDLG | 2/3 | yes | $2.12 \cdot 10^4$ | 60.2 |
| | 1/3 | no | $2.26 \cdot 10^3$ | 495.8 |

Using the proposed simplified model for expansion, one can investigate effects of shattered glass plies onto interlayers and adjacent undamaged plies. Figure 17 shows different strain patterns on the outer surface of the beam at varying stiffness of the interlayer material. These results can be correlated and validated with experimental measurements from strain gauges positioned on the outer surface of specimens.

Comparing readings in Figure 18 with the position of instruments, measurements appear to be consistent with a swiftly relaxing material: strain gauges $e11$ and $e15$, positioned at 50 $mm$ from the edge of the beam, have recorded considerably high strains at failure, but those readings are rapidly dropping in the first minutes.

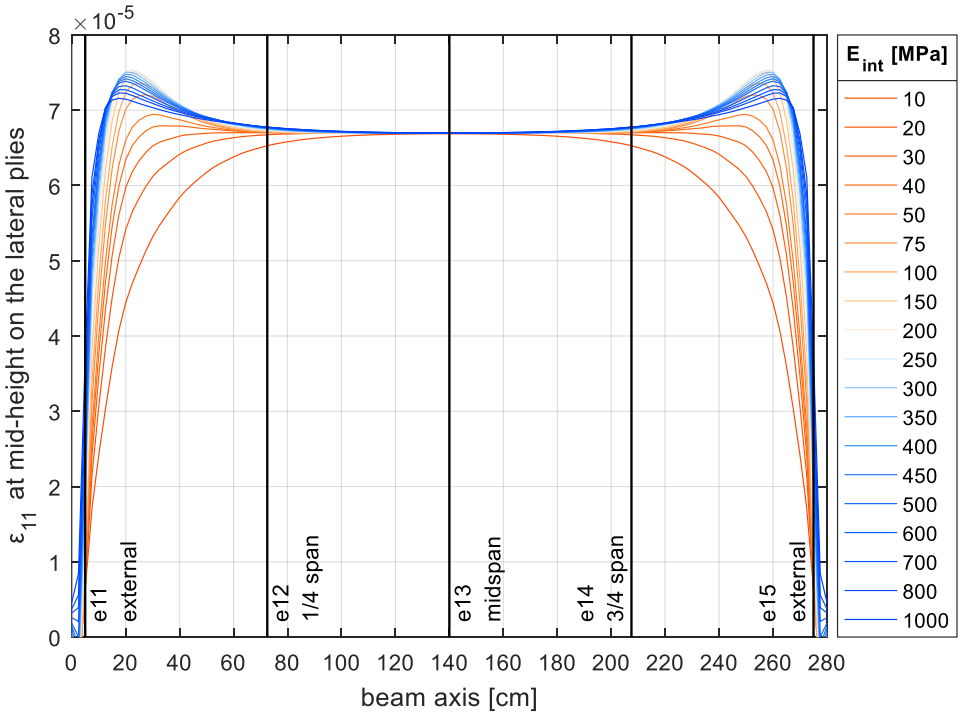


*Figure 17 – numerically calculated strain on the outer glass plies after failure of the central ply*

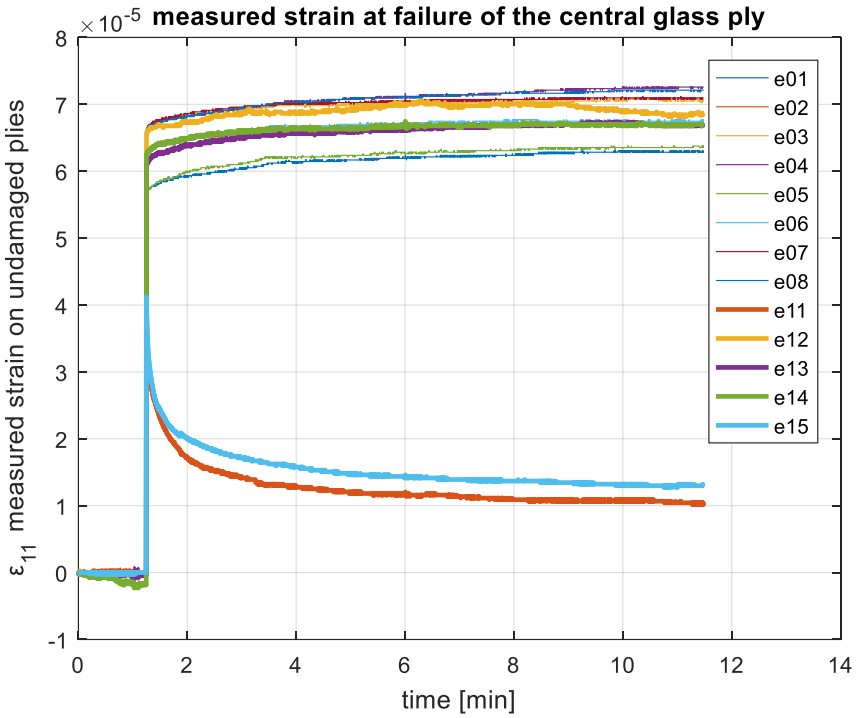


*Figure 18 – experimental strain on the outer glass plies after failure of the central ply*

Numerical results allow to investigate how shear stresses are transferred through the interlayer (Figure 19). Regardless the stiffness of the material, the shear transfer zone from the expanding central ply to the outer undamaged plies shows a striking peak between 50 and 100 *mm*, while the transfer zone progressively expands towards the inner regions at decreasing the shear modulus of the interlayer material.

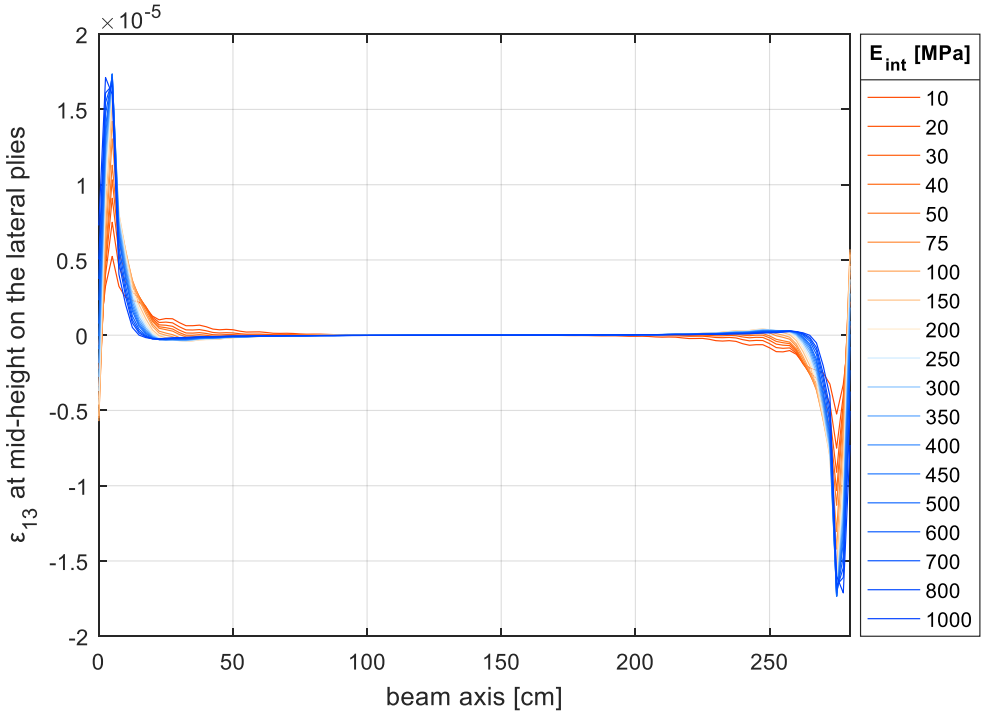


*Figure 19 – shear transfer trough the interlayer at failure of the central glass ply*

Measured strains at mid-span (strain-gauges *e*11 and *e*15 aside) increase in the first hour, and gradually drop over time (Figure 20).

After the failure of the central ply, a gradual reduction of recorded strain over time, like the one recorded after the first hour up to 24 hours in Figure 20, can be interpreted as the effect of the viscous deformations within the interlayer. Nonetheless, this phenomenon alone cannot explain the initial increase of strain that was recorded for a brief amount of time (about 1hr), just after the failure of the ply (Figure 18 and Figure 20). Once the failure of the ply occurs, most cracks are generated almost instantly. However, experimental observations showed that the number and density of cracks progressively grows over a short amount of a few hours. Initially, when the glass fails, the interlayer exhibits a strong action in holding back the fragments. As the time passes, the interlayer viscous deformations originate a progressive drop in its ability to clasp the fragments and containing cracks from expanding. As a result, new cracks form over time and contribute to the overall expansion of the fractured ply. From a macroscopic point of view, this behavior results in a delayed expansion that for DG41 interlayer has shown not to be completely negligible for the first hour, regardless the thickness of the interlayer.

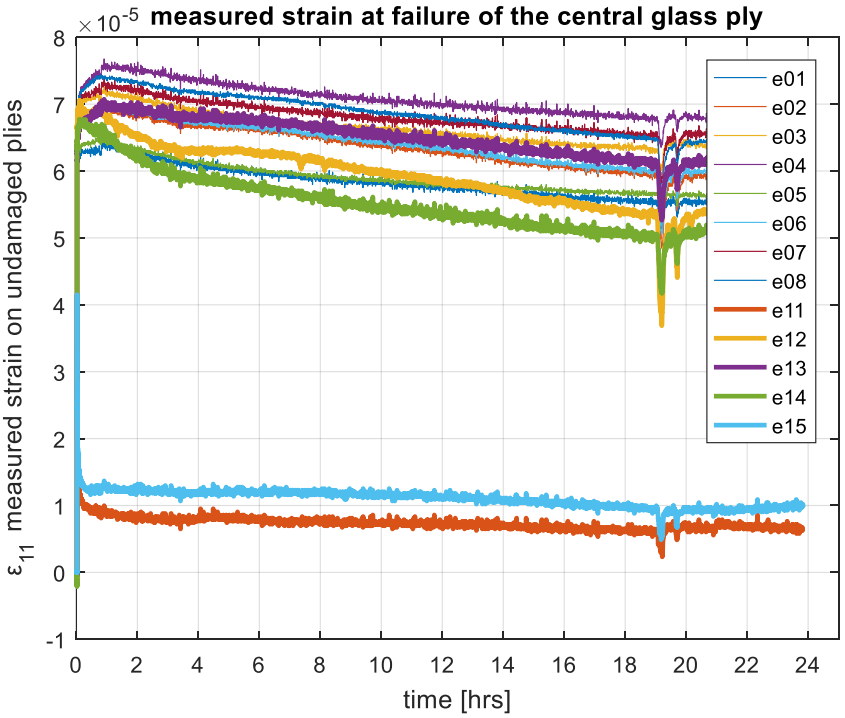


*Figure 20 – long-term monitoring of the strain-gauges upon failure of the central glass ply*

The thermal expansion model can also be used to study non-symmetrical damage states with two broken plies. By using data listed in

Table 5, insight on the lateral deflection can be obtained and compared with experimental measurements. Looking at results of the numerical model, a decrease of the interlayer's stiffness, that accounts for viscous relaxation of the interlayer material, do not produce significant variations of the overall accumulated deflection along the axis. While the model shows a progressively diminishing sag, experimental measurements show a slight increase (Figure 21). This inconsistency may be explained by considering that the model does not consider the above-mentioned delayed increase in the number of cracks, which effectively contributes to expanding the lateral and central broken plies and consequently induces a further sag increase.

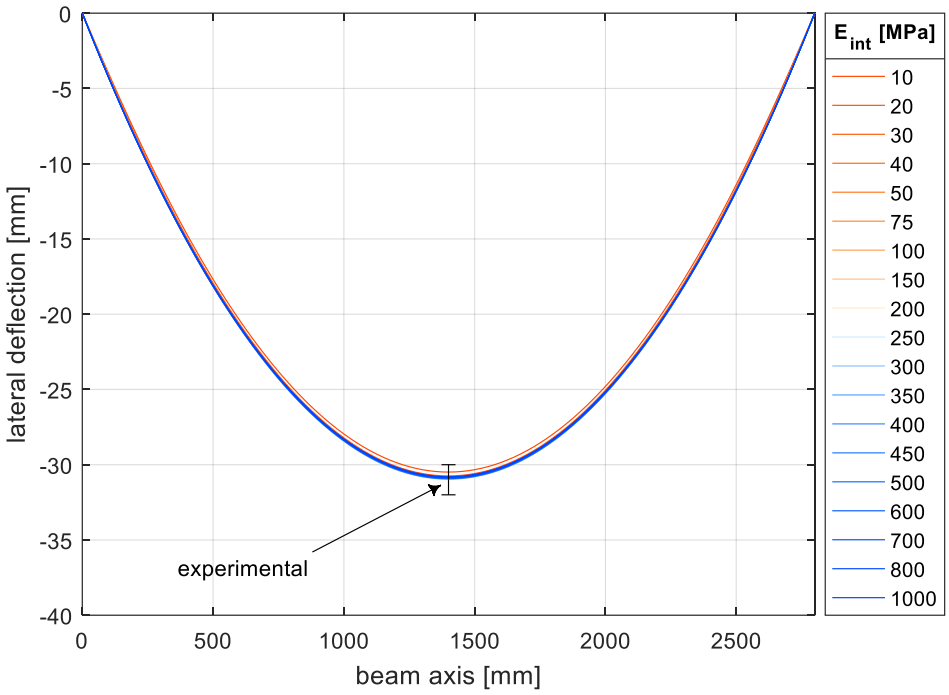


*Figure 21 – numerical lateral deflection of the beam at failure of the lateral ply for varying $E_{int}$ compared to experimental measurements. View from above*

After the conclusion of tests, specimens have been stored outside the laboratory and have therefore been subjected to usual environmental conditions: moderate exposure to sun and wind, seasonal precipitations and icing, with temperatures ranging approximately between -5 °C and 40 °C. Thus, long-term effects have been observed (Figure 22). After six months of storage, while the DG*x* laminates had completely lost the original shape, the polycarbonate reinforcements inserted in DGM*x* specimens allowed for the shape to be almost completely hold. Moreover, the limited deformation of the latter also reduced penetration of moisture and rainfall inside cracks, allowing for a significantly higher adhesion of fragments to develop. While fragments of DG beams could be easily removed just swiping the hand over the beams, fragments of DGM beams were still firmly adherent to the interlayer.


*Figure 22 – long-term effects of usual outdoor environmental conditions on FDLG*

Table 6 presents general information that can be useful from a designer point of view to understand and compare effects of progressive damage on LG elements.

*Table 6 – noteworthy effects of progressive damage on LG beams*

| | **2x1.52 mm DG41-LG** | **2x3.04 mm DG41-LG with PC** |
|---|---|---|
| **ULG** | | |
| Influence of the interlayer for in-plane bending | negligible | negligible |
| **Symmetrical PDLG** | | |
| Longitudinal expansion | limited† | limited† |
| Lateral deflection | none | none |
| Longitudinal tensile stresses on undamaged plies | non-negligible | non-negligible |
| Influence of the interlayer for in-plane bending | negligible | negligible |
| Relaxation rate of tensile stresses after failure | very slow | slow |
| **Asymmetrical PDLG** | | |
| Longitudinal expansion | limited or null‡ | Limited or null‡ |
| Lateral deflection | non-negligible | non-negligible |
| Longitudinal tensile stresses on undamaged plies | negligible | negligible |
| Rotation at the end supports | non-negligible | non-negligible |
| Influence of the interlayer for in-plane bending | negligible | small |
| Relaxation rate of tensile stresses after failure | very slow | slow |
| **FDLG** | | |
| Influence of the interlayer for in-plane bending | limited | considerable |
| Long-term ability to preserve the shape | very limited | good |
| Long-term fragments adhesion | very limited | good |

† generally negligible, provided there are no stiff constraints to elongation at both ends of the beam,
‡ because of the significant lateral deflection, the longitudinal relative displacement of beam ends can result in a net contraction rather than an elongation.

**Conclusions**

The bending response of three-plies LG beams with DG41 interlayer and reinforced-DG41 interlayer was investigated. While the base unreinforced version consisted in two 1.52mm thick interlayers, the reinforced version was created using two 3.06mm thick strata of DG41, being each stratum reinforced with an embedded thin polycarbonate foil (0,2 *mm* thick). Tests were carried out for increasing levels of damage, from the undamaged state to the fully damaged state.

Tests were performed to investigate effects of damaged glass plies on the response of the composite LG material. To this end, two aspects showed to be relevant:

- a beneficial effect in terms of "tension stiffening",
- a detrimental effect due to induced tensile stresses and transversal sag on undamaged plies.

The contribution of shattered glass plies to the overall stiffness of beams was investigated and compared to undamaged plies: results are given in terms of equivalent elastic moduli of glass.

Tests showed that shattered glass plies still contribute to the stiffness of PDLG specimens with polyvinyl interlayer thanks to a tension-stiffening effect, like it was found for ionoplast-laminated elements in a previous research. The expansion of tempered glass at failure was investigated, and a simple model to simulate the expansion in LG beams is proposed and validated.

Tests also highlight benefits of a polycarbonate foil embedded in the interlayer matrix; those benefits proved to be relevant mainly for the highest levels of damage. When all glass plies fail, the presence of a thin polycarbonate foil gives both higher flexural capacity and allows for the shape to be hold for a substantial amount of time. This insight is important in designing LG structural elements that are hard to replace and therefore need to be carefully evaluated when they are fully damaged and subjected to long-term loads.

**Acknowledgements**

The authors gratefully acknowledge Novavetro S.r.l. for the financial support to the research; Mr. Saverio Giordano, Mr. Enzo Barlacchi and Mr. Franco Bruni (Laboratory of Structures and Materials, DICEA) for execution of tests.

**References**

[1] Joel J. Global Structural Glazing 2016 Industry Trends, Sales, Supply, Demand, Analysis & Forecast to 2021. 2016 n.d.
[2] Transparency Market Research. Construction Glass Market - Global Industry Analysis, Size, Share, Trends and Forecast. 2016.
[3] Mihir J, Prabodh P, Shaan K. Flat Glass Industry At A Glance. 2015.
[4] Bennison SJ, Qin MH, Davies PS. High-performance laminated glass for structurally efficient glazing. Innov Light Struct Sustain Facades 2008:1–12.
[5] Ledbetter SR, Walker AR, Keiller AP. Structural use of glass. J Archit Eng 2006;12:137–49. doi:10.1061/(ASCE)1076-0431(2006)12:3(137).
[6] Barsom JM. Fracture of Tempered Glass. J Am Ceram Soc 1968;51:75–8. doi:10.1111/j.1151-2916.1968.tb11840.x.
[7] Louter C, Belis J, Veer F, Lebet J-P. Durability of SG-laminated reinforced glass beams: Effects of temperature, thermal cycling, humidity and load-duration. Constr Build Mater 2012;27:280–92. doi:10.1016/j.conbuildmat.2011.07.046.
[8] ISO-12543-4. Laminated glass and laminated safety glass. Part 4: Test methods for durability. vol. 44. 2012.
[9] Ensslen F. Influences of weathering on the durability of laminated safety glass.pdf. ISAAG - Int. Symp. Appl. Archit. Glas., 2006, p. 183–94.
[10] Cagnacci E, Orlando M, Spinelli P. Il vetro come materiale strutturale. Polistampa; 2010.
[11] Consiglio Nazionale Delle Ricerche. CNR-DT 210/2013 Istruzioni per la Progettazione, l'Esecuzione ed il Controllo di Costruzioni con Elementi Strutturali di Vetro 2013.
[12] Biolzi L, Cagnacci E, Orlando M, Piscitelli LR, Rosati G. Long-term response of glass-PVB double-Lap joints. Compos Part B 2014;63:41–9.
[13] Pagano NJ. Stress fields in composite laminates. Int J Solids Struct 1978;14:385–400. doi:10.1016/0020-7683(78)90020-3.
[14] Minor JE, Reznik PL. Failure Strengths of Laminated Glass. J Struct Eng 1990;116:1030–9. doi:10.1061/(ASCE)0733-9445(1990)116:4(1030).
[15] Duser A Van, Jagota A, Bennison SJ. Analysis of Glass/Polyvinyl Butyral Laminates Subjected to Uniform Pressure. J Eng Mech 1999;125:435–42. doi:10.1061/(ASCE)0733-9399(1999)125:4(435).
[16] Soules TF, Busbey RF, Rekhson SM, Markovsky A, Burke MA. Finite-Element Calculation of Stresses in Glass Parts Undergoing Viscous Relaxation. J Am Ceram Soc 1987;70:90–5. doi:10.1111/j.1151-2916.1987.tb04935.x.
[17] Biolzi L, Orlando M, Piscitelli LR, Spinelli P. Static and dynamic response of progressively damaged ionoplast laminated glass beams. Compos Struct 2016;157. doi:10.1016/j.compstruct.2016.09.004.
[18] Tripathy AR, Chen W, Kukureka SN, MacKnight WJ. Novel poly(butylene terephthalate)/poly(vinyl butyral) blends prepared by in situ polymerization of cyclic poly(butylene terephthalate) oligomers. Polymer (Guildf) 2003;44:1835–42. doi:10.1016/S0032-3861(03)00029-6.
[19] Vallabhan CVG, Das YC, Magdi M, Asik M, Bailey JR. Analysis of Laminated Glass Units. J Struct Eng 1993;119:1572–85. doi:10.1061/(ASCE)0733-9445(1993)119:5(1572).
[20] Alvarez G, Flores JJ, Aguilar JO, Gómez-Daza O, Estrada CA, Nair MTS, et al. Spectrally selective laminated glazing consisting of solar control and heat mirror coated glass: preparation, characterization and modelling of heat transfer. Sol Energy 2005;78:113–24. doi:10.1016/j.solener.2004.06.021.
[21] Louter C. Metal-to-glass bonding properties of an acrylate adhesive (DELO GB368) and an ionoplast interlayer (SentryGlas) at 23 , -20 and 60 ° C. Glas Perform Days 2009 2009:139–43.
[22] Dhaliwal AK, Hay JN. The characterization of polyvinyl butyral by thermal analysis. Thermochim Acta 2002;391:245–55.
[23] Galuppi L, Royer-Carfagni G. The design of laminated glass under time-dependent loading. Int J Mech Sci 2013;68:67–75. doi:10.1016/j.ijmecsci.2012.12.019.
[24] Aklonis JJ, Shaw MT, William MJ. Introduction to polymer viscoelasticity. vol. 59. 1972.

doi:10.1016/j.matchar.2007.05.008.
[25] Duser A Van, Jagota A, Bennison SJ. Analysis of Glass/Polyvinyl Butyral Laminates Subjected to Uniform Pressure. J Eng Mech 1999;125:435–42. doi:10.1061/(ASCE)0733-9399(1999)125:4(435).
[26] Behr RA, Minor JE, Norville HS. Structural Behavior of Architectural Laminated Glass. J Struct Eng 1993;119:202–22. doi:10.1061/(ASCE)0733-9445(1993)119:1(202).
[27] Behr RA, Minor JE, Linden MP. Load Duration and Interlayer Thickness Effects on Laminated Glass. J Struct Eng 1986;112:1441–53. doi:10.1061/(ASCE)0733-9445(1986)112:6(1441).
[28] Feirabend S, Sobek W. Bewehrtes Verbundsicherheitsglas. Stahlbau 2008;77:16–22. doi:10.1002/stab.200810027.
[29] Louter C. Bewehrte Glasträger. Stahlbau 2008;77:23–7. doi:10.1002/stab.200810028.
[30] Ivanov I V. Analysis, modelling, and optimization of laminated glasses as plane beam. Int J Solids Struct 2006;43:6887–907. doi:10.1016/j.ijsolstr.2006.02.014.
[31] Foraboschi P. Behavior and Failure Strength of Laminated Glass Beams. J Eng Mech 2007;133:1290–301. doi:10.1061/(ASCE)0733-9399(2007)133:12(1290).
[32] Cagnacci E, Orlando M, Spinelli P. Experimental campaign and numerical simulation of the behaviour of reinforced glass beams. Glas. Perform. Days, Tampere, Finland: 2009, p. 484–7.
[33] BS EN 572-9:2004 Glass in building. Basic soda lime silicate glass products. Evaluation of conformity/Product standard. 2004.
[34] DIN 53457 (1987-10) Testing Of Plastics; Determination Of The Elastic Modulus By Tensile, Compression And Bend Testing. 1987.
[35] International ASTM. ASTM D638-14, Standard Test Method for Tensile Properties of Plastics. West Conshohocken, PA: 2014. doi:10.1520/D0638-14.
[36] Dassault Systèmes. ABAQUS Documentation. 2011th ed. Providence, RI, USA: n.d.
[37] Timoshenko S. History of Strength of Materials: With a Brief Account of the History of Theory of Elasticity and Theory of Structures. Dover Publications; 1953.
[38] Bansal NP, Doremus RH. Handbook of Glass Properties. Elsevier Science; 2013.